GEOPHYSICAL RESEARCH LETTERS, VOL. 30, NO. 5, 1211, DOI:10.1029/2002GL016409, 2003

Hybrid simulations of the expanding solar wind: Temperatures and drift velocities

Petr Hellinger and Pavel Trávníček

Institute of Atmospheric Physics, AS CR, Prague, Czech Republic

André Mangeney and Roland Grappin

Observatoire de Paris, Meudon, France

We study the evolution of the expanding solar wind using a one-dimensional and a two-dimensional expanding box model [*Grappin et al.*, 1993] implemented here within a hybrid code [*Liewer et al.*, 2001]. We first consider a plasma with protons and 5 % of alpha particles, without drift between the protons and alphas, considering successively the low-beta and high-beta cases. Then we consider a strong drift between protons and alphas, again separately the low-beta and high-beta case. Without drift, the evolution of the low-beta plasma is adiabatic. In the high-beta plasma without drift, the fire hose instabilities disrupt the adiabatic evolution. Finally, with a drift, the adiabatic evolution is stopped by the oblique Alfvén instability and the parallel magnetosonic instability for low-beta plasma and for high-beta plasma, respectively. The two instabilities slow down the alphas and heat alphas and protons.

1. Introduction

The fast solar wind shows three distinct features: it expands in the transverse directions as it moves in the radial direction; it contains an important wave turbulence; finally, the particle distribution function is far from being Maxwellian. Temperature anisotropies and particle beams are commonly observed in the solar wind. Moreover heavy ions, as alpha particles, are usually hotter and move faster than the solar wind protons [*Marsch et al.*, 1982a, b; *Reisenfeld et al.*, 2001]. The ion behavior in the fast solar wind is largely nonadiabatic: the adiabatic invariant $T_\perp/B$ is not conserved, $T_\perp$ being the perpendicular temperature. The departure from adiabatic behavior could be caused by several effects: the interaction of ions with the solar wind turbulence [*Hu and Habbal*, 1999; *Gary et al.*, 2001], the appearance of local instabilities driven by drift velocities between protons and heavy ions [*Li and Habbal*, 2000; *Gary et al.*, 2000, and references therein] and/or by temperature anisotropies [*Gary et al.*, 1998; *Hellinger and Matsumoto*, 2000].

In this paper we study the evolution of the expanding plasma using a one-dimensional (1-D) and a two-dimensional (2-D) expanding box model implemented here within a hybrid code (section 2). We first consider a plasma with protons and 5 % of alpha particles, without drift between the protons and alphas, considering successively the low-beta and high-beta cases (section 3). Then we consider a strong drift between protons and alphas, again separately the low-beta and high-beta case (section 4). We discuss the results and compare them with *in situ* observations (section 5).

2. Hybrid expanding box model

In this paper we use a modified version of a 1-D and 2-D hybrid code [*Matthews*, 1994]: a Hybrid Expanding Box (HEB) code. The HEB code is an implementation of the expanding box model used in magnetohydrodynamic context by *Grappin et al.* [1993] to study the effects of plasma expansion on the wave evolution. The 1-D and 2-D HEB codes are similar to the 1-D HEB code by *Liewer et al.* [2001] and was developed independently. The HEB code models the expansion as a linearly driven evolution. One assumes a solar wind with a constant velocity U. The physical lengths $\boldsymbol{x}_r$ varies as $\boldsymbol{x}_r = \mathcal{L}\boldsymbol{x}$ where $\mathcal{L}$ is a diagonal matrix with $\mathcal{L}_{11} = 1, \mathcal{L}_{22,33} = 1 + t/t_e$ and t_e is a characteristic time of the expansion, $t_e = R_0/U$ where R_0 is the initial distance from the Sun. The code solves the evolution of the system in the coordinates $\boldsymbol{x}$ and $\boldsymbol{v}$ co-moving with the expansion. The physical velocities $\boldsymbol{v}_r$ are $\boldsymbol{v}_r = \mathcal{L}\boldsymbol{v}$. The equation of the movement for an ion with charge q and mass m reads:

$$d\boldsymbol{x}/dt = \boldsymbol{v}, \quad d\boldsymbol{v}/dt = q/m(\mathcal{L}^{-1}\boldsymbol{E} + \mathcal{L}^{-2}\boldsymbol{v} \times \tilde{\boldsymbol{B}}) - 2\dot{\mathcal{L}}\mathcal{L}^{-1}\boldsymbol{v}.$$

The effective magnetic field $\tilde{\boldsymbol{B}}$ in these coordinates evolves with the physical electric field $\boldsymbol{E}$ as $\partial\tilde{\boldsymbol{B}}/\partial t = -\mathrm{rot}(\mathcal{L}\boldsymbol{E})$ and is related to the physical magnetic field by $\boldsymbol{B} = \mathcal{L}\tilde{\boldsymbol{B}}/\det\mathcal{L}$. The electric field $\boldsymbol{E}$ is given as $\boldsymbol{E} = (\mathrm{rot}\boldsymbol{B}\times\boldsymbol{B}/\mu_0 - \boldsymbol{J}_i\times\boldsymbol{B} - \mathrm{grad}p_e)/(en)$, where μ_0 is the magnetic permeability of vacuum, n is the physical electron number density, a sum over different ion species, $en = \sum q/\det\mathcal{L}\int f d^3\boldsymbol{v}$, $\boldsymbol{J}_i$ is the ion current, a sum over different ion species, $\boldsymbol{J}_i = \sum q/\det\mathcal{L}\int \mathcal{L}\boldsymbol{v} f d^3\boldsymbol{v}$, and p_e is the electron pressure $p_e = nk_BT_e$ (k_B is Boltzman constant and T_e is the electron temperature; electrons are assumed to be isothermal).

Units of space and time are c/ω_{pi0} and Ω_{i0}, respectively, where c is the speed of light, $\omega_{pi0} = \sqrt{n_0e^2/m_p\epsilon_0}$ is the initial proton plasma frequency, and $\Omega_{i0} = eB_0/m_p$ is the initial proton gyrofrequency (B_0 is the initial magnitude of $\boldsymbol{B}$, n_0 is the initial density, e and m_p are the proton electric charge and mass, respectively; finally, ϵ_0 is the dielectric permitivity of vacuum). The codes use a spatial resolution dx, dy and there are N_p particles per cell. Fields and moments are defined on a 1-D and 2-D grid with dimensions n_x and $n_x \times n_y$, respectively. The exact values of dx, dy, N_p, n_x, and n_y will be given in the text. The time step for the particle advance is $dt = 0.05\Omega_{i0}^{-1}$, while the magnetic field $\boldsymbol{B}$ is advanced with a smaller time step $dt_B = dt/4$ for all the simulations.

3. Plasma without alpha-proton drift

A homogeneous slowly expanding plasma (without any fluctuating wave energy) evolves adiabatically. The ion parallel and perpendicular temperatures $T_{||}$ and $T_\perp$ satisfy the CGL equations $T_\perp \propto B$ and $T_{||} \propto n^2/B^2$, respectively. In the case of a strictly radial expansion, $\boldsymbol{B}(0) = (1, 0, 0)$, the temperature anisotropy evolves as $T_{p\perp}/T_{p||} \propto (1 + t/t_e)^{-2}$.

3.1. Low-beta protons

We perform 1-D and 2-D HEB simulations starting with an initially low proton beta $\beta_p = 0.1$ and a characteristic expansion time

0094-8276/05/2002GL016409$5.00

$t_e = 2000$ for a time interval $\Delta t = 4000$. The 1-D simulation had $dx = 0.5$, $N_p = 1024$, $n_x = 512$, while the 2-D simulation had $dx = dy = 1$, $N_p = 256$, $n_x = n_y = 256$. During the time period $\Delta t = 4000$ the evolution of the two 1-D and 2-D systems was adiabatic and at the end of the simulation we observe a strong proton temperature anisotropy $T_{p\perp}/T_{p||} = 1/9$. In the low-beta case, the plasma is stable. Indeed, electromagnetic instabilities, driven by the proton temperature anisotropy, needs a substantial proton beta [*Gary et al.*, 1998; *Hellinger and Matsumoto*, 2000]. Adding 5% of alpha particles ($\beta_{||\alpha} = 0.01$) does not change much the results.

3.2. High-beta protons

We now perform 1-D and 2-D HEB simulations starting with high-beta protons ($\beta_{p||} = 1$) that are already anisotropic: $T_{p\perp}/T_{p||} = 0.5$; the anisotropic proton plasma is at the beginning stable. Other parameters are identical to those used in section 3.1. During the expansion the plasma evolves adiabatically and the ratio $T_{p\perp}/T_{p||}$ decreases. In the 1-D simulation, the parallel fire hose instability *Gary et al.* [1998] appears later on, and stops this decrease. The system then evolves around marginal stability. In the 2-D simulation, the parallel fire hose instability appears as well, but soon after its appearance the oblique fire hose instability appears [*Hellinger and Matsumoto*, 2000]. The essentially non-quasilinear evolution of oblique fire hose [*Hellinger and Matsumoto*, 2001] leads to an important increase of $T_{p\perp}/T_{p||}$ and a decay of wave activity. The system returns to a nearly adiabatic evolution and the parallel and oblique fire hose reappear. The system oscillates between stability and marginal stability.

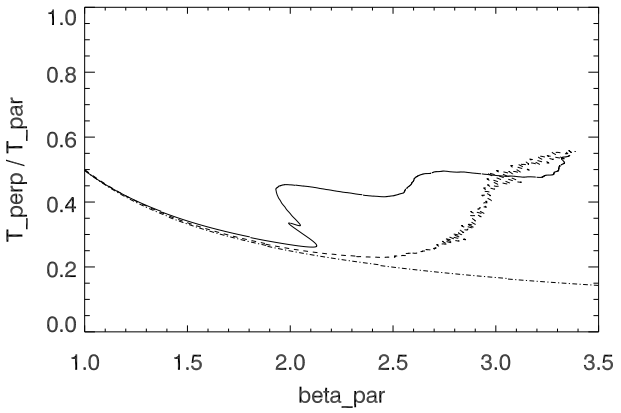

Figure 1. High-beta, pure protons plasma: Evolution in the space ($\beta_{p||}$, $T_{p\perp}/T_{p||}$) for (dashed) 1-D simulation and for (solid) 2-D simulation. The adiabatic prediction is is denoted by the dash-dotted curve.

Figure 1 shows the evolution of the two simulations in the 2-D space ($\beta_{p||}$, $T_{p\perp}/T_{p||}$). The solid and dashed curves show the evolution of the 2-D and 1-D simulations, respectively. The dashed-dotted curve shows the adiabatic prediction. Figure 1 clearly shows the initial adiabatic evolution for the two simulations and the appearance of instabilities later on. The anisotropy $T_{p\perp}/T_{p||}$ stops around 0.25 for the 1-D simulation and slowly increases with $\beta_{p||}$ [*Gary et al.*, 1998]. The 2-D evolution is different, the $T_{p\perp}/T_{p||}$ rapidly increases from 0.3 to about 0.5 and then again decreases, nearly adiabatically. The instabilities then set up again and all the evolution repeats twice, however with smaller excursions in the ($\beta_{p||}$,$T_{p\perp}/T_{p||}$) space. Adding 5% of alpha particles ($\beta_{||\alpha} = 0.05$) does not change much the results, but the increase of $T_{p\perp}/T_{p||}$ due to the fire hose instabilities is lower, at the expense of heating the alpha particles.

4. Plasma with a strong alpha-proton drift

In situ observations in the solar wind shows that the alpha particles travel faster than protons and the drift velocity between the two populations is about the local Alfvén velocity. Let us now look at the consequences of this drift. We investigate low-beta and high-beta plasmas with the number density of alpha particles 5% of the number density of electrons and with a strong alpha-proton drift.

4.1. Low-beta plasma

In this section we study the evolution of the expanding plasma for low-beta protons and alpha particles with $\beta_{||p} = 0.1$ and $\beta_{||\alpha} = 0.03$. The 2-D simulation has $dx = dy = 2$, $n_x = 256$, $n_y = 128$, and number of particles per cell: $N_{pp} = 128$ for protons and $N_{\alpha p} = 64$ for alpha. In the expanding plasma, the radial velocities are constant. Therefore, during an adiabatic evolution, the radial drift velocity v_d is constant while the local Alfvén velocity v_A decreases. The ratio v_d/v_A thus increases and one expects ion-beam instabilities to appear [*Gary et al.*, 2000].

We start the simulation with the drift velocity $v_d = v_A$ and the characteristic time for the expansion $t_e = 1000$, corresponding to a wind speed twice that of Section 3. In this simulation, the dominant instability is left-handed, oblique Alfvén, resonant via cyclotron resonance [*Gary et al.*, 2000]. Figure 2 shows the evolution of the ratio between the drift velocity v_d and the local Alfvén velocity in the simulation (solid curve). The predicted adiabatic evolution is denoted by the dash-dotted curve.

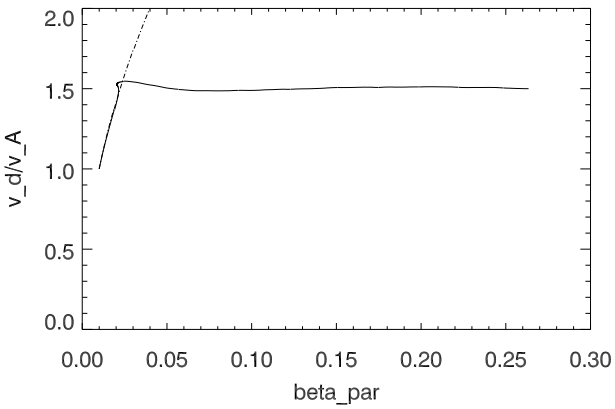

Figure 2. Low-beta plasma: alpha-proton drift velocity in units of the local Alfvén velocity (solid curve) as a function of $\beta_{\alpha||}$. The adiabatic prediction is denoted by the dash-dotted curve.

The oblique Alfvén instability strongly modifies the ion temperatures. This effect is illustrated in Figure 3 for protons (left panel) and for alpha particles (right panel). Figure 3 shows the evolution (solid curve) in the 2-D space of ($\beta_{p||}$,$T_{p\perp}/T_{p||}$) (left panel), and ($\beta_{\alpha||}$,$T_{\alpha\perp}/T_{\alpha||}$) (right panel). The dash-dotted curve shows the adiabatic prediction.

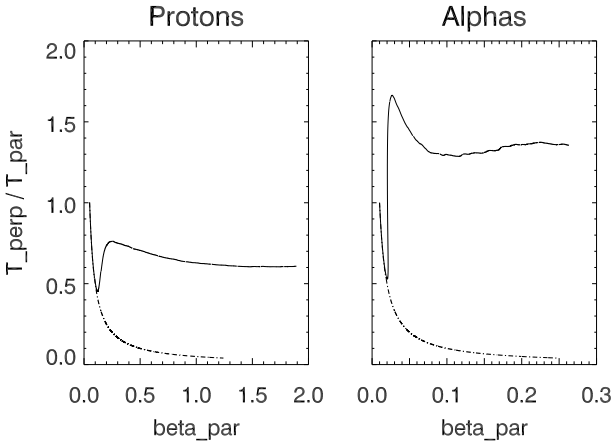

Figure 3. Low-beta plasma with drift: Evolution of protons (left panel) and alphas (right panel) in the space ($\beta_{p||}$, $T_{p\perp}/T_{p||}$) and ($\beta_{\alpha||}$, $T_{\alpha\perp}/T_{\alpha||}$), respectively. The adiabatic prediction is denoted by the dash-dotted curves.

Figure 3 clearly shows that the instability is able to stop the adiabatic cooling in the case of low-beta protons. The free energy from the drift velocity of alphas is transferred to perpendicular temperature of protons and alpha particles.

The growth rate of instabilities driven by the ion-beams strongly depends on plasma properties (temperatures and drift velocities), therefore, let us now finish this study with a case of relatively high-beta protons and alpha particles with a drift velocity.

4.2. High-beta plasma

In this section we study the evolution of the expanding plasma for high-beta protons and alpha particles $\beta_{||p} = 0.5$ and $\beta_{||\alpha} = 0.16$. Other parameters are identical to those used in the section 4.1. In this simulation the dominant instability is right-handed, magnetosonic, with maximum growth rate at parallel propagation, resonant via cyclotron resonance [*Gary et al.*, 2000]. Figure 4 shows the evolution of the ratio between the drift velocity v_d and the local Alfvén velocity in the simulation (solid curve). The predicted adiabatic evolution is denoted by the dash-dotted curve.

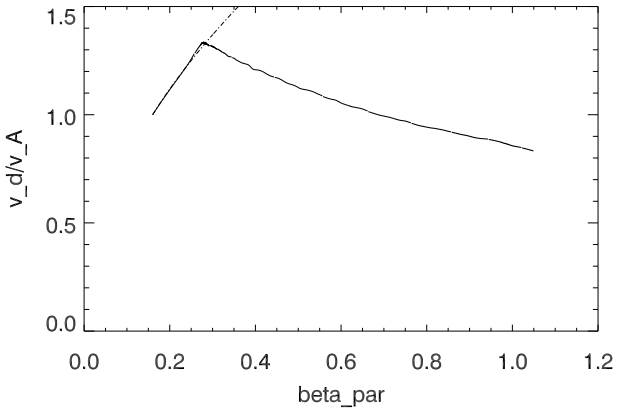

Figure 4. High-beta plasma: alpha-proton drift velocity in units of the local Alfvén velocity (solid curve) as a function of $\beta_{\alpha||}$. The adiabatic prediction is denoted by the dash-dotted curve.

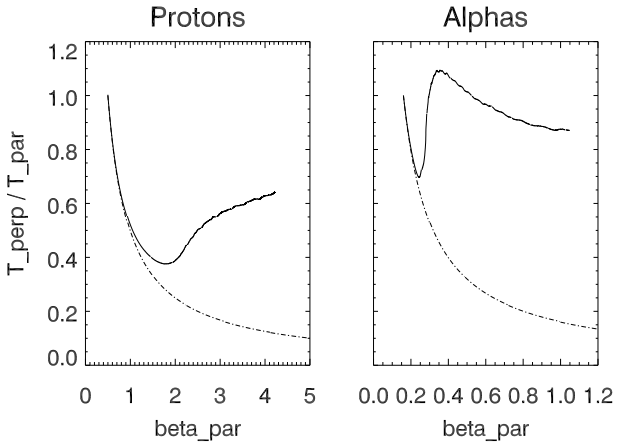

Figure 5. High-beta plasma with drift: Evolution of protons (left panel) and alphas (right panel) in the space ($\beta_{p||}$, $T_{p\perp}/T_{p||}$) and ($\beta_{\alpha||}$, $T_{\alpha\perp}/T_{\alpha||}$), respectively. The adiabatic prediction is denoted by the dash-dotted curves.

The magnetosonic instability strongly modifies the ion temperatures. This effect is illustrated in Figure 5 for protons (1eft panel) and for alpha particles (right panel). Figure 5 shows the evolution (solid curve) in the ($\beta_{p||}$,$T_{p\perp}/T_{p||}$) space (left panel) and the ($\beta_{\alpha||}$,$T_{\alpha\perp}/T_{\alpha||}$) space (right panel). The dash-dotted curve shows the adiabatic prediction.

5. Discussion and Conclusion

We have presented results of a recently developed simulation technique: a HEB code. We have applied this tool to study the evolution of ion temperature anisotropies and a drift speed in a slowly (strictly radially) expanding plasma. In the low-beta plasma case without drift between alphas and protons, the evolution of the system is double adiabatic (CGL) and important ion temperature anisotropies appear. In the high-beta plasma case without drift between alphas and protons, the plasma evolves at the beginning adiabatically, and later on, the parallel fire hose appears. In 1-D simulations, the waves generated by the instability keep the system around marginal stability with an anticorrelation between the proton anisotropy $T_{p||}/T_{p\perp}$ and the proton parallel beta $\beta_{p||}$ [*Gary et al.*, 1998]. In 2-D simulations, the oblique fire hose becomes dominant and the evolution departs from marginal stability

[*Hellinger and Matsumoto*, 2001]. The results of these simulations are in a good agreement with linear theory and with previous simulation studies that used standard hybrid codes [*Gary et al.*, 1998; *Hellinger and Matsumoto*, 2000, 2001].

However, these results are not applicable to the physics of fast solar wind, where an important drift velocity between protons and alphas exists. The inclusion of a drift between protons and alphas strongly changes the plasma behavior. In a low-beta plasma, the dominant mode is an oblique left-handed mode [*Gary et al.*, 2000, and references therein]. In this case, when the instability develops, the drift velocity is continuously slowed down so that it remains 1.5 times local Alfvén velocity. The generated waves heat protons and alphas preferably in the perpendicular directions. This heating compensates the adiabatic cooling of protons and alphas. The proton temperature anisotropy is $T_{p||}/T_{p\perp} \sim 0.6$ while the alpha temperature anisotropy is $T_{\alpha||}/T_{\alpha\perp} \sim 1.3$ in later stages of the evolution. Our low-beta simulation with a strictly radial magnetic field corresponds to the polar regions below 1 AU for typical fast solar wind parameters. For these distances there are only observations by Helios [*Marsch et al.*, 1982a, b], however, in the ecliptic plane. The results of the HEB code are only in a partial agreement with these observations. The drift velocity is comparable to the local Alfvén velocity, however observations show that the drift velocity is usually smaller than the local Alfvén velocity.

In the high-beta plasma case, we observe a slightly different behavior. In this case the dominant instability is the magnetosonic one and this instability is able to importantly decelerate alphas and heat protons and alphas. The ratio between drift velocity and the local Alfvén velocity decreases with $\beta_{\alpha||}$, and, at the later stages of the simulations, the drift velocity is smaller than the local Alfvén velocity. The proton temperature anisotropy is $T_{p||}/T_{p\perp} \sim 0.6$ and has a tendency to increase while the alpha temperature anisotropy is $T_{\alpha||}/T_{\alpha\perp} \sim 0.9$ and decreases with $\beta_{\alpha||}$. These results are in good qualitative agreement with high latitude Ulysses observations of *Reisenfeld et al.* [2001] of higher beta plasma at 2–5 AU that show an anticorrelation between the proton temperature and the ratio between the drift velocity and the local Alfvén speed, with the drift velocity being below the local Alfvén speed. Also the observed anisotropy $T_{\alpha||}/T_{\alpha\perp} \sim 0.7$ is not far from what the HEB simulation shows. However, the observed proton anisotropy is $T_{p||}/T_{p\perp} > 1$.

In conclusion, a HEB simulation shows a trajectory in parameter space (along the marginal stability path and departures from it) induced by the expansion, which could be approximatively traced by many standard hybrid simulations [*Gary et al.*, 2000, and reference therein]. This trajectory represents self-consistently the effect of a slow expansion on the plasma properties. The results are in a good agreement with linear theory and standard hybrid simulations [*Li and Habbal*, 2000; *Gary et al.*, 2000]. The comparison with observations shows many points of agreement, both on the pressure anisotropies and the proton-alpha drift. Future work will be devoted to study the influence of the initial plasma parameters, the impact of the transverse components of the mean magnetic field and also to a detailed comparisons between observations and HEB simulations.

Acknowledgments. The authors thank the CIAS at Meudon Observatory for hospitality during summer 2001 and 2002 (MHD workshop) and acknowledge the grants PICS 1175 and GA AV B3042106.

References

Gary, S. P., H. Li, S. O'Rourke, and D. Winske, Proton resonant firehose instability: Temperature anisotropy and fluctuating field constraints, *J. Geophys. Res.*, *103*, 14,567–14,574, 1998.

Gary, S. P., L. Yin, D. Winske, and D. B. Reisenfeld, Alpha/proton magnetosonic instability in the solar wind, *J. Geophys. Res.*, *105*, 20,989–20,996, 2000.

Gary, S. P., B. E. Goldstein, and J. T. Steinberg, Helium ion acceleration and heating by Alfvén/cyclotron fluctuations in the solar wind, *J. Geophys. Res.*, *106*, 24,955–24,964, 2001.

Grappin, R., M. Velli, and A. Mangeney, Nonlinear-wave evolution in the expanding solar wind, *Phys. Rev. Lett.*, *70*, 2190–2193, 1993.

Hellinger, P., and H. Matsumoto, New kinetic instability: Oblique Alfvén fire hose, *J. Geophys. Res.*, *105*, 10,519–10,526, 2000.

Hellinger, P., and H. Matsumoto, Nonlinear competition between the whistler and Alfvén fire hoses, *J. Geophys. Res.*, *106*, 13,215–13,218, 2001.

Hu, Y. Q., and S. R. Habbal, Resonant acceleration and heating of solar wind ions by dispersive ion cyclotron waves, *J. Geophys. Res.*, *104*, 17,045–17,056, 1999.

Li, X., and S. R. Habbal, Proton/alpha magnetosonic instability in the fast solar wind, *J. Geophys. Res.*, *105*, 7483–7489, 2000.

Liewer, P. C., M. Velli, and B. E. Goldstein, Alfvén wave propagation and ion cyclotron interaction in the expanding solar wind: One-dimensional hybrid simulations, *J. Geophys. Res.*, *106*, 29,261–29,281, 2001.

Marsch, E., K. H. Muhlhauser, H. Rosenbauer, R. Schwenn, and F. M. Neubauer, Solar-wind helium-ions – observations of the Helios solar probes between 0.3-AU and 1-AU, *J. Geophys. Res.*, *87*, 35–51, 1982a.

Marsch, E., K. H. Muhlhauser, R. Schwenn, H. Rosenbauer, W. Pilipp, and F. M. Neubauer, Solar-wind protons – 3-dimensional velocity distributions and derived plasma parameters measured between 0.3-AU and 1-AU, *J. Geophys. Res.*, *87*, 52–72, 1982b.

Matthews, A., Current advance method and cyclic leapfrog for 2D multispecies hybrid plasma simulations, *J. Comput. Phys.*, *112*, 102–116, 1994.

Reisenfeld, D. B., S. P. Gary, J. T. Gosling, J. T. Steinberg, D. J. McComas, B. E. Goldstein, and M. Neugebauer, Helium energetics in the high-latitude solar wind: Ulysses observations, *J. Geophys. Res.*, *106*, 5693–5708, 2001.

P. Hellinger and P. Trávníček, Institute of Atmospheric Physics, Prague 14131, Czech Republic. (petr.hellinger@ufa.cas.cz; trav@alenka.ufa.cas.cz)

A. Mangeney and R. Grappin, Observatory of Paris, Meudon 92190, France. (mangeney@despace.obspm.fr; roland.grappin@obspm.fr)